

# JOINT TRANSPORTATION RESEARCH PROGRAM

INDIANA DEPARTMENT OF TRANSPORTATION  
AND PURDUE UNIVERSITY



## Development of an Intelligent Snowplow Truck that Integrates Telematics Technology, Roadway Sensors, and Connected Vehicle



**Justin Mahlberg, Yaguang Zhang, Sneha Jha, Jijo K. Mathew,  
Howell Li, Jairaj Desai, Woosung Kim, Jeremy McGuffey, Tim  
Wells, James V. Krogmeier, Darcy M. Bullock**

## **RECOMMENDED CITATION**

Mahlberg, J., Zhang, Y., Jha, S., Mathew, J. K., Li, H., Desai, J., Kim, W., McGuffey, J., Wells, T., Krogmeier, J. V., & Bullock, D. M. (2021). *Development of an intelligent snowplow truck that integrates telematics technology, roadway sensors, and connected vehicle* (Joint Transportation Research Program Publication No. FHWA/IN/JTRP-2021/27). West Lafayette, IN: Purdue University. <https://doi.org/10.5703/1288284317355>

## **AUTHORS**

### **Justin Mahlberg**

Graduate Research Assistant  
Lyles School of Civil Engineering  
Purdue University

### **Yaguang Zhang**

Post-Doctoral Research Assistant  
School of Electrical and Computer Engineering  
Purdue University

### **Sneha Jha**

Graduate Research Assistant  
School of Electrical and Computer Engineering  
Purdue University

### **Jijo K. Mathew, PhD**

Transportation Research Engineer  
Lyles School of Civil Engineering  
Purdue University

### **Howell Li**

JTRP Senior Software Engineer  
Lyles School of Civil Engineering  
Purdue University

### **Jairaj Desai**

Graduate Research Assistant  
Lyles School of Civil Engineering  
Purdue University

## **JOINT TRANSPORTATION RESEARCH PROGRAM**

The Joint Transportation Research Program serves as a vehicle for INDOT collaboration with higher education institutions and industry in Indiana to facilitate innovation that results in continuous improvement in the planning, design, construction, operation, management and economic efficiency of the Indiana transportation infrastructure.  
[https://engineering.purdue.edu/JTRP/index\\_html](https://engineering.purdue.edu/JTRP/index_html)

Published reports of the Joint Transportation Research Program are available at <http://docs.lib.purdue.edu/jtrp/>.

## **NOTICE**

The contents of this report reflect the views of the authors, who are responsible for the facts and the accuracy of the data presented herein. The contents do not necessarily reflect the official views and policies of the Indiana Department of Transportation or the Federal Highway Administration. The report does not constitute a standard, specification or regulation.

## TECHNICAL REPORT DOCUMENTATION PAGE

<b>1. Report No.</b> FHWA/IN/JTRP-2021/27	<b>2. Government Accession No.</b>	<b>3. Recipient's Catalog No.</b>	
<b>4. Title and Subtitle</b> Development of an Intelligent Snowplow Truck that Integrates Telematics Technology, Roadway Sensors, and Connected Vehicle		<b>5. Report Date</b> August 2021	
		<b>6. Performing Organization Code</b>	
<b>7. Author(s)</b> Justin Mahlberg, Yaguang Zhang, Sneha Jha, Jijo K. Mathew, Howell Li, Jairaj Desai, Woosung Kim, Jeremy McGuffey, Tim Wells, James V. Krogmeier, and Darcy M. Bullock		<b>8. Performing Organization Report No.</b> FHWA/IN/JTRP-2021/27	
<b>9. Performing Organization Name and Address</b> Joint Transportation Research Program Hall for Discovery and Learning Research (DLR), Suite 204 207 S. Martin Jischke Drive West Lafayette, IN 47907		<b>10. Work Unit No.</b>	
		<b>11. Contract or Grant No.</b> SPR-4322	
<b>12. Sponsoring Agency Name and Address</b> Indiana Department of Transportation (SPR) State Office Building 100 North Senate Avenue Indianapolis, IN 46204		<b>13. Type of Report and Period Covered</b> Final Report	
		<b>14. Sponsoring Agency Code</b>	
<b>15. Supplementary Notes</b> Conducted in cooperation with the U.S. Department of Transportation, Federal Highway Administration.			
<b>16. Abstract</b> The Indiana Department of Transportation (INDOT) manages and maintains over 28,000 miles of roadways. Maintenance of the roadways includes pavement repair in the summer and snow removal and de-icing in the winter. The prioritization of assets during winter storm events is crucial and impacts travel and safety. The objective of this project was to identify and develop tools INDOT could provide its operators to effectively perform winter operation de-icing activities. This project examined application methods and data to provide analytics and make data-driven decisions for state-wide deployment and operations. Discovery of calibration metrics partnered with fleetwide telematics enabled the development of analytic dashboards that allowed real-time evaluations and adjustments to be made during winter operation activities. These tools will allow the agency to better treat and enhance safety for road users.			
<b>17. Key Words</b> winter operations, calibration, brine application, telematics, probe data, de-icing, anti-icing, prescription maps, shadow detection, Indiana		<b>18. Distribution Statement</b> No restrictions. This document is available through the National Technical Information Service, Springfield, VA 22161.	
<b>19. Security Classif. (of this report)</b> Unclassified	<b>20. Security Classif. (of this page)</b> Unclassified	<b>21. No. of Pages</b> 33 including appendices	<b>22. Price</b>

## EXECUTIVE SUMMARY

### Motivation

The Indiana Department of Transportation (INDOT) manages and maintains over 28,000 miles of roadways. Maintenance of the roadways includes pavement repair in the summer as well as snow removal and de-icing in the winter. The prioritization of assets during winter storm events is crucial and impacts travel and safety. The objective of this project was to identify and develop tools for INDOT operators to effectively perform winter operation de-icing activities.

### Study

This project examined application methods and data to provide analytics and make data-driven decisions for state-wide winter operation deployment and operations. Discovery of calibration metrics partnered with fleetwide telematics enabled the development of analytic dashboards that allowed real-time evaluations and adjustments to be made during winter operation activities. These tools will allow the agency to better treat and enhance safety for road users. The advancement of a functioning automated brine applicator provided insight towards development of a functioning, intelligent snowplow.

### Results

The findings of this research were as follows.

1. Calibration of salt spreaders is important to ensure that the proper amount of salt is delivered to the roadway. The team developed and demonstrated new calibration techniques and methods, reducing the material usage and labor needed to calibrate granular de-icing equipment. Figure 1.1a shows the use of the new calibration box and Figure 1.1b illustrates the calibration workshops held at each district. The URL in Figure 1.1 shows a time-lapse at the Crawfordsville calibration workshop and the complete calibration of a truck (Mahlberg et al., 2021).
2. When anti-icing chemicals are applied to bridge decks, the driver must turn the application on and off at each bridge. One pass on a single lane in one direction requires the driver to turn the brine application on and off approximately 100 times (Figure 1.2a). Depending upon traffic and driver workload, some applications zones may be missed, so there is variation in the number of spray zones between runs (Table 1.1). The team developed and scaled an automated precision brine applicator on two 5,500-gallon tankers (Figure 1.2b) to reduce driver workload and the potential for distracted driving.

3. Effectively managing plow trucks during a winter storm requires having good knowledge of where the trucks are so that resources can be most effectively allocated. The project team successfully integrated telematics from 1,100 trucks into real-time dashboards. Figure 1.3a shows a time-space diagram (heatmap) colorized by speed for I-65 northbound direction between mile markers 200 and 262 from February 14th to February 16th, 2021. Snowplow trajectories are overlaid on the heatmap to show snow removal activities with respect to traffic speeds. Additionally, to provide context to winter operation procedures statewide, Figure 1.3b illustrates interstate traffic speeds, weather radar, truck locations, and applied materials on the roadway surfaces. A video of operations during the storm can be found in Figure 1.3. This dashboard allows operation managers to analyse storm impact and effectively deploy trucks. Figure 1.3c shows the interactive feature of the dashboard and the ability for the user to select a truck to determine location information and view the dash camera image. The URL in Figure 1.3 shows a time-lapse of plow deployment during the February 15th, 2021, winter storm (Sakhare et al., 2021).
4. Development of after-action winter storm reports to provide agencies with data-driven decisions and training. This information will provide agency management with insight on deployment and evaluation measures of each precipitation event. Figure 1.4a illustrates vehicle speeds operating below 45 mph on Indiana Interstates from January 18th to February 16th, 2021. Figure 1.4b shows the deployed snowplows during that same interval.
5. Generation of large-scale dynamic prescription maps for winter road treatment operations utilizing sun-shadow simulation. These prescription maps provide agencies with a tool to increase treatment efficiently, reduce environmental impact and prioritize high-risk road segments.

### Recommendations

1. Training and implementation of calibration practices should be continued to provide accurate data and ensure correct application amounts.
2. Continued implementation and installation of automated precision controllers fleetwide to reduce driver distraction and provide consistent pre-treatment measures.
3. Further testing and data validation with the telematic installer to ensure accurate data readings and evaluations.
4. Develop training materials to provide agency operators and managers tools to determine operation best-practices and deployment.
5. Perform simulation tests on larger road networks and include additional information including degree of shading, weather, and obstacle types to present more accurate sun radiation results.

## CONTENTS

1. PROJECT OVERVIEW . . . . .	1
1.1 Introduction . . . . .	1
1.2 Overview of Implementation . . . . .	1
2. CALIBRATION . . . . .	5
2.1 Development of the Calibration Box . . . . .	5
2.2 Calibration Implementation . . . . .	5
3. PRECISION BRINE APPLICATION . . . . .	6
3.1 Development of a Prototype . . . . .	6
3.2 Scaling to a 5,500-gallon Tanker . . . . .	7
4. WINTER OPERATIONS DASHBOARD . . . . .	8
4.1 Telematic Installation . . . . .	8
4.2 Telematic Dashboard Development . . . . .	8
4.3 Automated Granular Application . . . . .	11
5. WINTER PROBE DATA AFTER ACTION REPORTS . . . . .	11
6. AUTOMATED GENERATION OF BRINE PRESCRIPTION BASED ON SHADOW . . . . .	13
6.1 Motivation . . . . .	13
6.2 Direct-Path Blockage and Normalized Sun Energy . . . . .	13
6.3 Simulator Implementation . . . . .	15
6.4 Simulator Performance Evaluation . . . . .	16
6.5 Case Study for US 41 . . . . .	16
6.6 Conclusion . . . . .	19
7. RESULTS, SUMMARY, AND RECOMMENDATIONS . . . . .	19
REFERENCES . . . . .	20
APPENDICES	
Appendix A. Innovative Calibration Techniques . . . . .	22
Appendix B. Summary of Training Materials . . . . .	22

## LIST OF FIGURES

Figure	Page
<b>Figure 1.1</b> Calibration box utilization and training workshops	1
<b>Figure 1.2</b> Summary of application zones and 5,500-gallon tanker	2
<b>Figure 1.3</b> Integration of AVL data into real-time dashboards	3
<b>Figure 1.4</b> Winter after action congestion report for January 18th–February 16th, 2021, winter storm	3
<b>Figure 1.5</b> Spreader values from INDOT truck	4
<b>Figure 1.6</b> Precision brine prototype vehicle	4
<b>Figure 1.7</b> Integration of AVL data into real-time dashboards	4
<b>Figure 2.1</b> Development of a calibration box	5
<b>Figure 2.2</b> INDOT application controllers	6
<b>Figure 3.1</b> Adaption of precision spraying technology from agriculture industry	6
<b>Figure 3.2</b> Equipment adaptation on prototype vehicle	7
<b>Figure 3.3</b> Scaling the prototype to INDOT fleet vehicle	7
<b>Figure 3.4</b> Motivation for automating material application	8
<b>Figure 3.5</b> Summary of application zones	8
<b>Figure 4.1</b> INDOT truck with Parsons telematics installed	8
<b>Figure 4.2</b> INDOT truck locations (blue dots) with interstate traffic speeds and radar weather overlay during January 14th–15th, 2021 storm	9
<b>Figure 4.3</b> INDOT truck location with salt application trails during January 14th–15th, 2021 storm	10
<b>Figure 4.4</b> Active plow positions of INDOT trucks	10
<b>Figure 4.5</b> Automated granular application testing and deployment	11
<b>Figure 5.1</b> I-65 northbound interstate heatmap for February 14th–16th, 2021	12
<b>Figure 5.2</b> I-94 Tandem plowing activities	13
<b>Figure 6.1</b> Illustration of the direct-path blockage scenario	14
<b>Figure 6.2</b> Power computation and normalization based on solar zenith angles	14
<b>Figure 6.3</b> Block diagram of the sun-shadow simulator	15
<b>Figure 6.4</b> Block diagram of the sun-shadow simulator illustrations of the road segmentation and the grid generation procedures for US 41 on Google Maps (Google, n.d.c; plus code: FHWQ+HC Terre Haute, Indiana): (a) From the road name with start and end points of interest, the location sampler automatically locates the road, divides it into small segments, and creates a simulation grid for each segment. (b) Grid points to inspect for one example road segment (50-m long)	16
<b>Figure 6.5</b> Example photos of building shadows at different times before the sunset, together with simulated blockage status for the same area overlaid on Google Maps (Google, n.d.a; plus code: C3CG+PV West Lafayette, Indiana)	17
<b>Figure 6.6</b> Comparison between a satellite image from Google Maps (n.d.b) and blockage results from the simulator	18
<b>Figure 6.7</b> A set of low-resolution simulations to locate high-risk locations for the 38-km US 41 road segment between Terre Haute and Rockville, Indiana	18
<b>Figure 6.8</b> Normalized daily sun energy values overlaid on Google Maps	19
<b>Figure 6.9</b> Simulation results loaded into Google Earth (Google, 2021) for better user interactions	19

## LIST OF TABLES

Table	Page
<b>Table 1.1</b> Summary of I-465 Application	2

## LIST OF ACRONYMS

JTRP	Joint Transportation Research Program
INDOT	Indiana Department of Transportation
AVL	Automatic Vehicle Location
RTK	Real-Time Kinematics
CAN	Controller Area Network
MRMS	Multi Radar/Multi-Sensor
LoS	Line of Sight
NREL	National Renewable Energy Laboratory
USGS	United States Geological Services
SPA	Solar Position Algorithm
DSM	Digital Surface Model
CDF	Cumulative Distribution Function

## 1. PROJECT OVERVIEW

### 1.1 Introduction

The Indiana Department of Transportation (INDOT) makes a considerable investment each year in maintenance operations around the state. These operations span a wide spectrum of activities from asphalt patching and summer mowing to winter snow and ice removal which all share common logistical aspects: planning, execution, and control of personnel, machines, and materials to achieve a maintenance goal. The efficiency of maintenance operations may be dramatically improved by the application of modern communications, computation, and control technologies, which are now available at a reasonable cost. The impact of winter weather events on travel cannot be overstated. Even very small precipitation events with cold temperatures can dramatically reduce roadway speeds. These winter weather events also significantly increase crash rates. During a typical winter season, it is not uncommon to see up to 600 miles of interstate impacted during a major storm despite significant resources devoted to plowing and de-icing activities. Modern snowplows now have sophisticated hydraulic systems as well as advanced control and logging at 10-second resolution for geocoded material application rates and plow up/down status that can provide agencies with necessary feedback to provide better services and snow removal processes.

### 1.2 Overview of Implementation

INDOT has a fleet of over 1,100 winter operations trucks and spends up to \$60 M annually on snow removal and de-icing as part of their winter operation maintenance activities. Materials for treating, including granular salt and liquid brine, contribute towards a significant part of that budget. The efficient application of these materials with automated solutions for managing driver workload can significantly reduce operating costs and staff turnover.

#### 1.2.1 Calibration

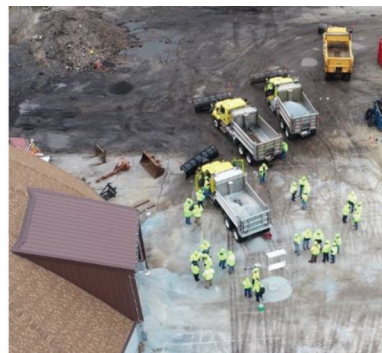
Capturing and evaluating salt application rates can provide insight to agencies on effective application techniques. Figure 1.5 shows the application rates from a truck during the January 12th, 2019, winter storm. Typical granular application rates range from 100–500 pounds per lane mile, but on January 12th and 13th, values were observed as high as 5,000 pounds per lane mile. Extreme values of this magnitude were observed in many of the fleet vehicles, generating discussion with controller manufacturers. Through testing and practice it was determined these values were due to uncalibrated controller systems.

#### 1.2.2 Precision Brine Application

Brine application has been shown to reduce salt usage by over 70% in winter operations compared to solid granular material (Breining, 2017). The efficient use of brine can reduce winter storm impacts, environmental impacts, and provide agencies with greater flexibility in resources and assets during a winter storm event (Fitch et al., 2013). Although brine is more effective than granular materials, the efficient application of material is difficult due to a shortage of experienced drivers. Agencies experience high turnover rates and the knowledge of application measures on a route may not be transferred to the next driver. Automating brine application reduces the turnover cost per employee in training time and resources and enhances a driver's ability to treat the driving surface efficiently and consistently regardless of their experience (Parker & Skitmore, 2005). Additionally, automating brine application reduces driver workload and distraction, making the process safer for the driver and other road users. Figure 1.6 shows the prototype that was developed to provide proof of concept and training to operators of the automation equipment and operation. Table 1.1 shows a summary of the applications completed on I-465 during the 2020–2021 winter season.



(a) Operator Utilizing the Calibration Box

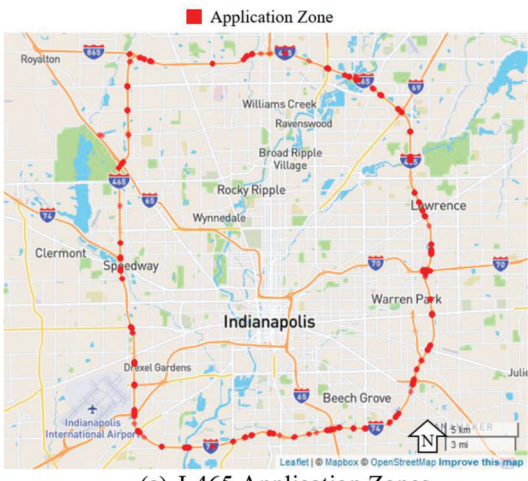


(b) La Porte Calibration Workshop

**Figure 1.1** Calibration box utilization and training workshops (see <https://doi.org/10.4231/XBET-8A88>).

TABLE 1.1  
Summary of I-465 Application

Date	# of Passes	# of Application Activations	Application Activations/Pass	Total App. Length (ft)	Application Length/Pass (ft)
11/12/2020	4 (1 IL, 3 OL)	395	98.8	136,353	34,000
11/17/2020	6 (3 IL, 3 OL)	647	107.8	268,054	44,700
01/11/2021	1 (1 IL)	51	51.0	31,546	31,546
03/02/2021	6 (3 IL, 3 OL)	437	72.8	182,851	30,475
<i>Total</i>		1,530	—	618,804	—



(a) I-465 Application Zones



(b) Leveraging Agriculture Technology to Brine Application

**Figure 1.2** Summary of application zones and 5,500-gallon tanker.

### 1.2.3 Winter Operations Dashboard

Data on the severity of the storm, temperature, wind conditions and the behavior of the storm combined with the use of AVL data reporting real-time position of fleet, can provide agencies with insight on performance measures during a winter storm event (Nixon & Qiu, 2005). Installation of telematic devices provided information from the vehicles Controller Area Network (CAN) port, including vehicle speed, odometer readings, and total vehicle running hours. The telematic devices also provided material application rates, GPS coordinates, and camera images at 1-minute frequencies.

Integrating the telematic data from snowplows with weather radar and traffic speeds provides transportation agencies with a tool to actively monitor storm

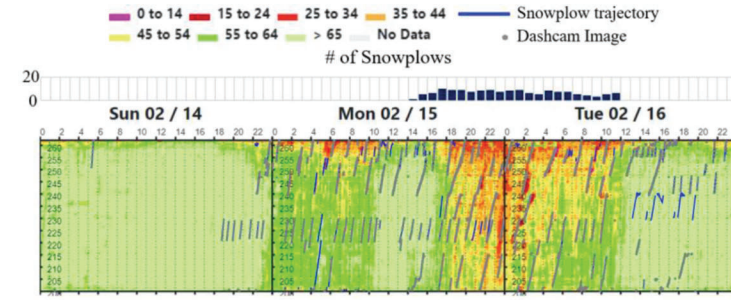
impact and deployment measures. Figure 1.7a illustrates the traffic speed, truck locations and applied materials on the roadway surfaces to provide context to winter operation procedures statewide. Figure 1.7b is a truck in callout *i* of Figure 1.7a and demonstrates the interactive feature of the dashboard and the ability for the user to select a truck to determine location information and view the dash camera image. The URL shows a time-lapse as the storm progresses through the state. This provides INDOT management the ability to observe current road conditions and make real-time decisions on application amounts and fleet deployment (Sakhare et al., 2021).

### 1.2.4 Winter Probe Data After Action Reports

Over 8,000 fatalities occur each year in the United States due to adverse road weather conditions (FHWA, 2020). Documentation and analysis from adverse weather events can provide agencies with performance metrics to better prepare for adverse weather conditions. Utilizing the data acquired through the AVL systems, the impact of winter storms on interstates was monitored over the winter 2020–2021 season. Performance metrics were based on congestion profiles (vehicle speeds operating below 45 mph) during a winter storm event (Brennan et al., 2013; Day et al., 2016). Figure 1.4a shows the congestion profile from January 18th to February 16th, 2021, stacked by INDOT districts. The largest impact was the winter storm that began late in the evening on the February 14th (callout *i*). The interstate system did not fully recover until 1:00 PM on February 16th. The greatest impact of the storm was at 9:30 PM on the February 15th with over 1,500 miles of interstate traveling at speeds less than 45 mph. Figure 1.4b shows the number of trucks deployed during each storm. During the storm on February 15th anywhere between 50–600 trucks were deployed statewide, except between 12:00–13:00 hours where shift changes were performed, and trucks went offline temporarily.

### 1.2.5 Automated Generation of Brine Prescription Based on Shadow

INDOT considers snow and ice removal as their number one priority during the winter (INDOT, 2021). Besides mechanical means, pre- and post-treatments of the road for anti- and de-icing are also among the most



(a) I-65 Northbound Heatmap with Snowplow Trajectories

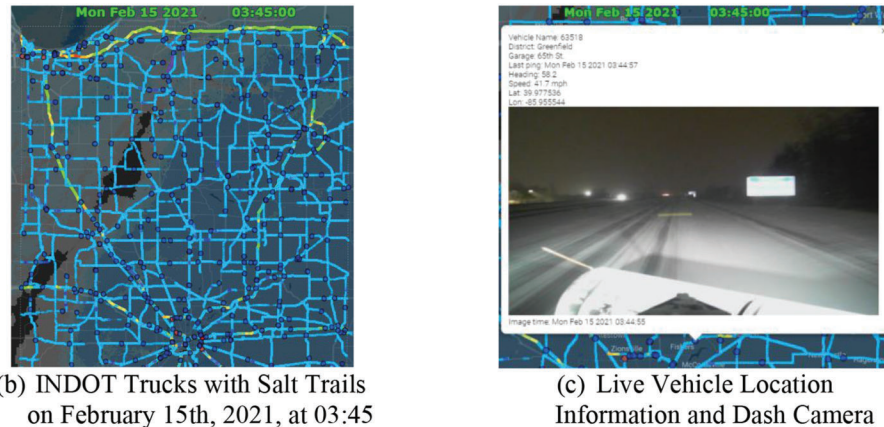


**Figure 1.3** Integration of AVL data into real-time dashboards (see <https://doi.org/10.4231/R3XJ-0875>).

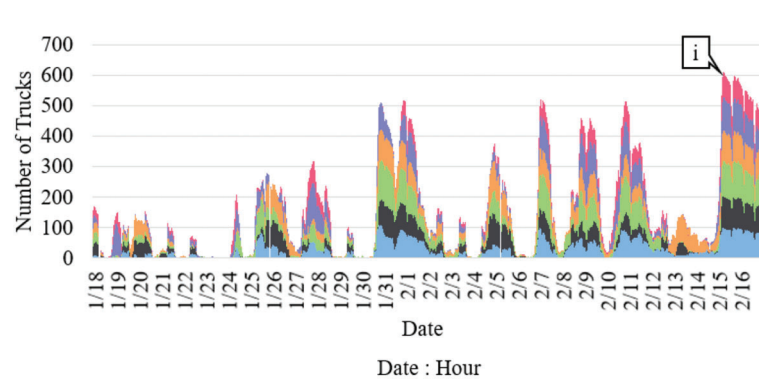
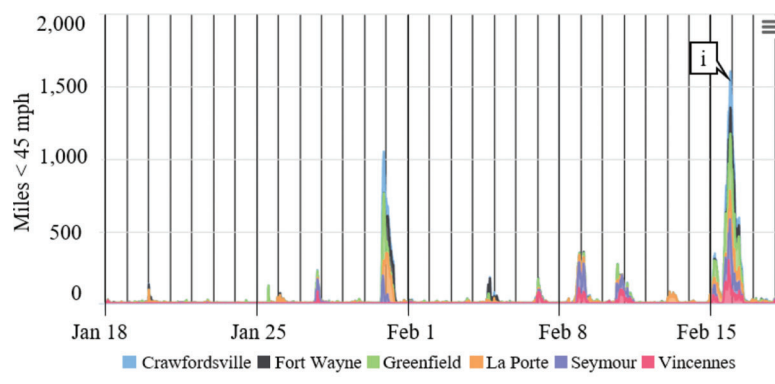


**Figure 1.4** Winter storm after action report for January 18th–February 16th, 2021.

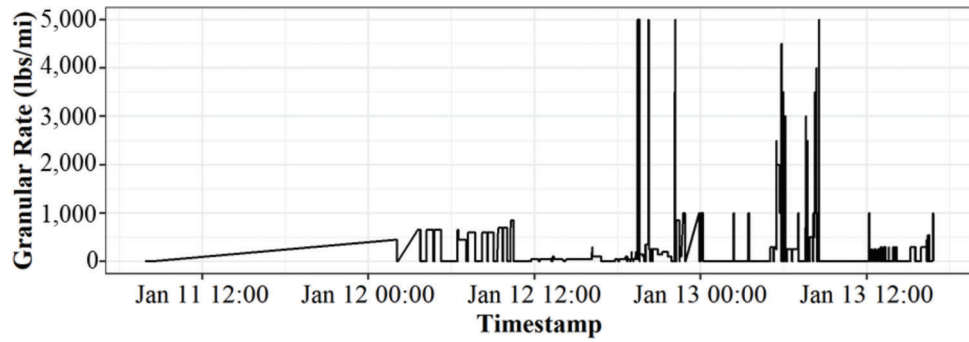


**Figure 1.5** Spreader values from INDOT truck.



**Figure 1.6** Precision brine prototype vehicle.

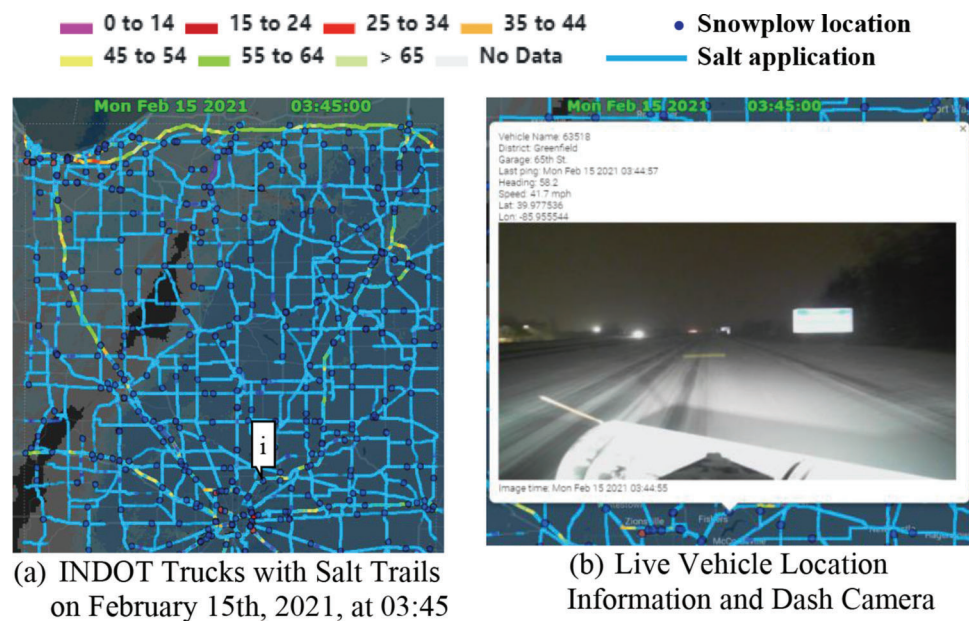


**Figure 1.7** Integration of AVL data into real-time dashboards (see <https://doi.org/10.4231/R3XJ-0875>).

effective measures. However, it is common practice today to apply treatments such as brine solutions and various chlorides evenly over long road segments,

although it has been long established that road surface in the shade suffers the snow and ice problem significantly more than that under the sun (Bogren &

Gustavsson, 1989; Bogren et al., 2000; Millory & Humphreys, 1969; Shao & Lister, 1995). A sun-shadow simulator to generate prescription maps for winter road treatment operations was developed to reduce the areas most affected by shade. This simulation provides agencies with a tool to increase treatment efficiently, reduce environmental impact and prioritize high-risk road segments.

## 2. CALIBRATION

A critical aspect of effective and efficient application of salt is a properly calibrated spreader system. Calibration of salt spreaders ensures the proper amount of salt is delivered to the roadway. Preliminary investigation found that trucks were offloading excess salt (around 50% more) before calibration. In the past, spreaders were often calibrated using scales to measure the weight of material off-loaded during a measured time interval. Although this method is accurate, it can be quite time consuming if scales are not on site or if material is collected on a tarp and weighed.

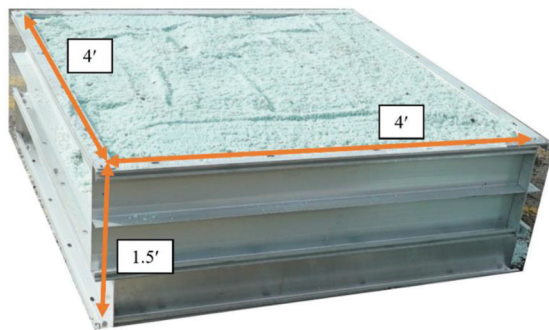
### 2.1 Development of the Calibration Box

The development of a volumetric based calibration procedure was necessary to reduce calibration time and make the process more feasible for agencies. Figure 2.1 shows the product, a bottomless calibration box constructed out of aluminum sign backing that holds a known volume (and weight). The calibration procedure

consists of calibrating the spreader and auger, offload amount, and speed component. The time-consuming aspect of calibration is the offload calibration, which includes determining the weight of the truck before and after offload and inputting the offloaded amount into the controller. This process can take upwards of 1–2 hours, but the calibration box eliminates the need for weighing the truck, allowing agencies to calibrate a truck in less than 10 minutes. A set of calibration tables can also be used to allow for variance in salt moisture content and densities. Results from repeated tests showed that calibrating improved the offloading inaccuracies by 30%, which could yield a significant reduction in costs and material usage. A one-page user guide that was developed to assist agencies with the calibration procedure can be found in Appendix A.

### 2.2 Calibration Implementation

Further training was provided to include different manufacturer controllers installed across the state (Figure 1.1a). Overall, the calibration workshops had over 200 participants. In 2020, the INDOT fleet was calibrated before the winter season through the provided training (Figure 1.1b). Training videos and supplementary material were created for four spreader types including the Muncie Advantage+ (Figure 2.2a), Certified Power Freedom 2 (Figure 2.2b), Muncie Omni (Figure 2.2c), and the FORCE America 5100ex (Figure 2.2d). Links to the training videos can be found in Appendix B.



$$\text{Volume of Calibration Box} = 1.5' \times 4' \times 4' = 24 \text{ ft}^3$$

$$\text{Assumed Density of Salt} = 80 \frac{\text{lb}}{\text{ft}^3}$$

$$\text{Approximate Weight of Salt in Bin} = 24 \text{ ft}^3 \times 80 \frac{\text{lb}}{\text{ft}^3} = 1,920 \text{ lbs}$$

**Figure 2.1** Development of a calibration box.



**Figure 2.2** INDOT application controllers.

### 3. PRECISION BRINE APPLICATION

The development of an automated brine application system for de-icing and pretreatment during winter operations was successfully implemented and tested during the project. The system leverages existing precision Real-Time Kinematic (RTK) technology used for spraying chemicals in the agriculture industry to control brine application (Figure 3.1) (Van Sickle, 2021). Examples of the controllers used can be seen in Figure 3.1 (Raven Applied Technology, 2020).

This innovation allows agencies to remotely send a prescription map with application zones and their rates to the in-cab operator. The system will automatically turn on/off the application at the prescribed rate when the vehicle enters/exits the application zones. In addition to material savings by preventing double application on previously applied areas, the system enables multiple vehicles to work

on the same brine route. This improves efficiency and using the real-time job sync, prevents application that other operators may have already captured. On job completion, the system generates a report highlighting the application areas and their rates, which agencies can use for after-action analysis to better manage material usage and assess winter maintenance operations.

#### 3.1 Development of a Prototype

Figure 3.2 shows the prototyped system on an electric utility vehicle (for campus roads and urban sidewalks) before scaling it up on a 5,500-gallon brine tanker capable of treating interstates and major arterials. Callout *i* is the cellular receiver for RTK correction, callout *ii* is the user interface and callout *iii* is the GPS receiver. Callout *iv* is the 100-gallon brine tank and callout *v* is the spray bar.



**Figure 3.1** Adaption of precision spraying technology from agriculture industry.



**Figure 3.2** Equipment adaptation on prototype vehicle.



(a) Scaling to 5,500-gallon Brine Tanker



(b) Equipment Adaptation on 5,500-gallon Brine Tanker

**Figure 3.3** Scaling the prototype to INDOT fleet vehicle.

### 3.2 Scaling to a 5,500-gallon Tanker

After successful deployment of the prototype, the team equipped the technology on a 5,500-gallon brine tanker. Figure 3.3b shows the adaption of the brine tanker. Callout *i* shows the left spray channel, callout

*ii* shows the right spray channel and callout *iii* shows the center spray channel. The side channels allow application on multiple lanes and coverage of merge/diverge lanes and exit ramps.

#### 3.2.1 Driver Workload and Varying Road Conditions

Advantages of this technology includes safety enhancement, reduction of driver workload, and efficient application of brine. Figure 3.4a and Figure 3.4b reveals some of the distractions that are presented to drivers. While operating the vehicle, the driver needs to focus on brine application, surrounding vehicles and operating the application controls. This system eliminates two of the higher driver workload activities by having the controller manage the application rate in each area, allowing the driver to maneuver the vehicle safely. Additionally, the application files can be programmed to account for areas that experience low-sunlight, higher winds, and other weather conditions (Figure 3.4c and Figure 3.4d).

#### 3.2.2 Application Log Reports

When examining the log reports, it was found that one pass on a single lane in one direction requires the driver to manually turn on and off the brine application approximately 100 times (Figure 3.5). Depending on the traffic and driver workloads, it is possible that some application zones can be missed, thus leading to uneven application rates between runs and drivers.

Table 1.1 shows a summary of the applications completed on I-465 during the 2020–2021 winter season. In only four applications there were over 1,500 application activations and over 113 miles of bridge decks and underpasses treated with brine. The variation between application length is dependent on traffic and driver workload. This system has been installed on two 5,500-gallon tankers to reduce driver workload and plans for future deployment are underway.



(a) Traffic Congestion during Operation



(b) Operator Controller



(c) Wet Pavement



(d) Blowing Snow Conditions

**Figure 3.4** Motivation for automating material application.

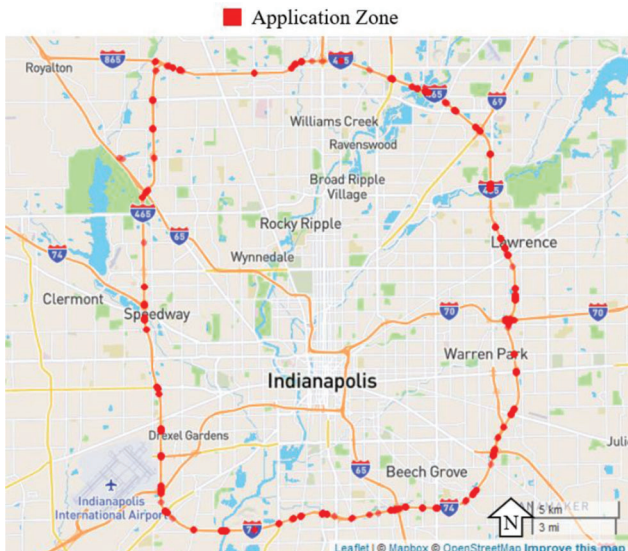


**Figure 3.5** Summary of application zones.

## 4. WINTER OPERATIONS DASHBOARD

### 4.1 Telematic Installation

Automatic Vehicle Location (AVL) systems were first implemented in public transportation for fleet management. As the technology evolved, the systems have been deployed on commercial fleets, emergency and security vehicles, and continue to be implemented on different agency vehicles (Hounsell & McLeod, 1998). For fleet management and training, AVL communication was installed on 1,100 INDOT fleet

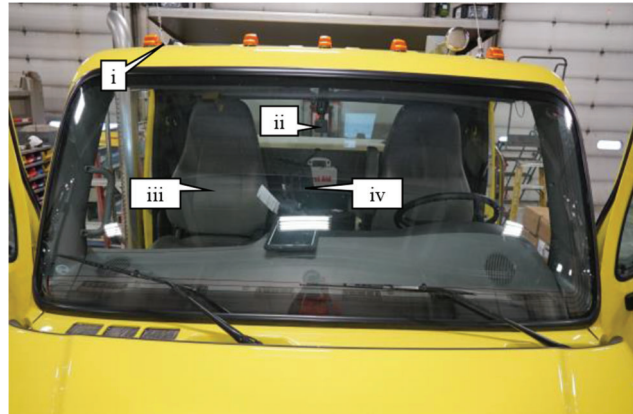


**Figure 4.1** INDOT truck with Parsons telematics installed.

trucks beginning in October 2021. Figure 4.1 shows the installed telematics on the vehicle. Callout *i* is the cellular antenna, callout *ii* is the dash camera on the vehicle, which captures an image every minute, callout *iii* is the AVL processor which is located behind the passenger seat, and callout *iv* is the AVL interface tablet. The system provides real-time vehicle location, controller and vehicle data, and dash images every minute, allowing agencies to actively monitor and deploy their assets.

### 4.2 Telematic Dashboard Development

Supplementary measures were used to evaluate and assess the road conditions and active deployment of snowplows. Figure 4.2b illustrates forecasted Multi-Radar/Multi-Sensor (MRMS) data from the national

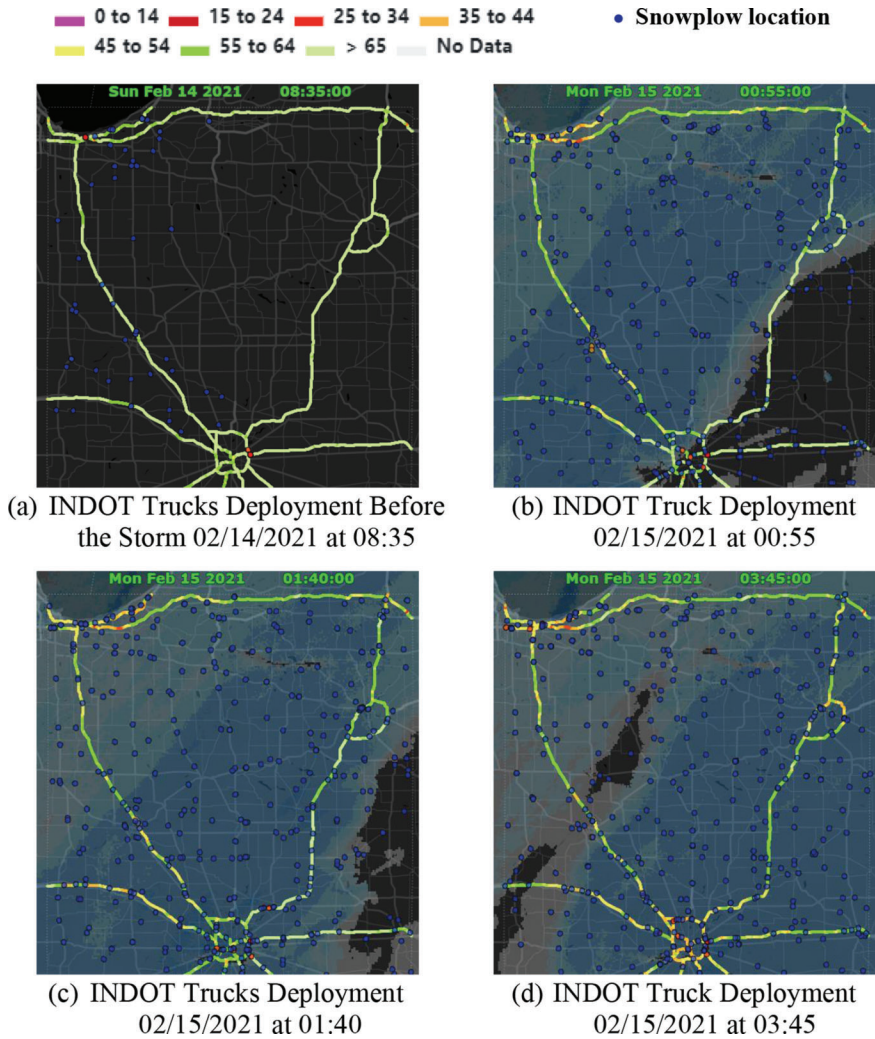


**Figure 4.2** INDOT truck locations (blue dots) with interstate traffic speeds and radar weather overlay during January 14th–15th, 2021 storm (see <https://doi.org/10.4231/R3XJ-0875>).

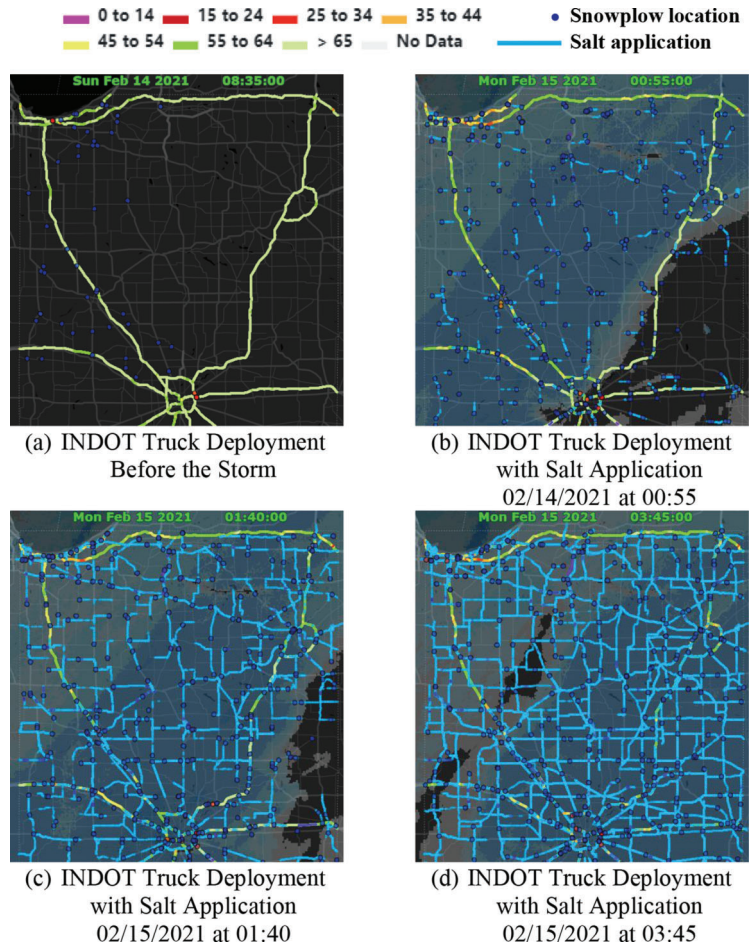
severe storm laboratory, and truck locations to provide context to winter operation procedures statewide. As previously shown, there is an interactive feature to view the current vehicle analytics and dash camera image. This provides agencies and operation managers the ability to observe current road conditions and make real-time decisions on application amounts and fleet deployment.

Figure 4.2 illustrates the dashboard showing the location of trucks (blue markers), current interstate speeds and radar weather overlay as the storm progresses. Around 8 AM, before the storm hits the state, there were 81 trucks actively monitoring the storm and accumulation (Figure 4.2a). Figure 4.2b shows there were over 500 trucks actively plowing while the storm progresses through the state. Figure 4.2c and Figure 4.2d show that as the storm moves further across the state more trucks are actively deployed to perform winter snow removal and de-icing activities.

Figure 4.3 presents similar information as Figure 4.2, with the addition of salt material application trails on

the graphic. It can be seen in Figure 4.3b that at 12:55 AM on February 15th, salt material began to be applied to the roadway surface. As the storm progressed, more routes had material applied (Figure 4.3c and Figure 4.3d). A video showing snowplow activity of the complete storm can be found in Appendix B. This dashboard allows agencies to analyze the impact of the storm and systematically allocate resources to manage the roadways.

Distinction between monitoring activities and active plowing status during a snowstorm event can provide further information on forecasted/radar precipitation and actual ground accumulation. This information is gathered from the hydraulic manifold sensor on the truck. Figure 4.4a shows the truck's hydraulic manifold that controls the plow, dump box, and augers/conveyor belt. Callout *i* shows the pressure sensor that detects the plow status. Figure 4.4b shows the validation of the sensor reading through the dash camera and validates the plow position sensor reading. Figure 4.4c shows the position of the plow when actively plowing.



**Figure 4.3** INDOT truck location with salt application trails during January 14th–15th, 2021 storm.

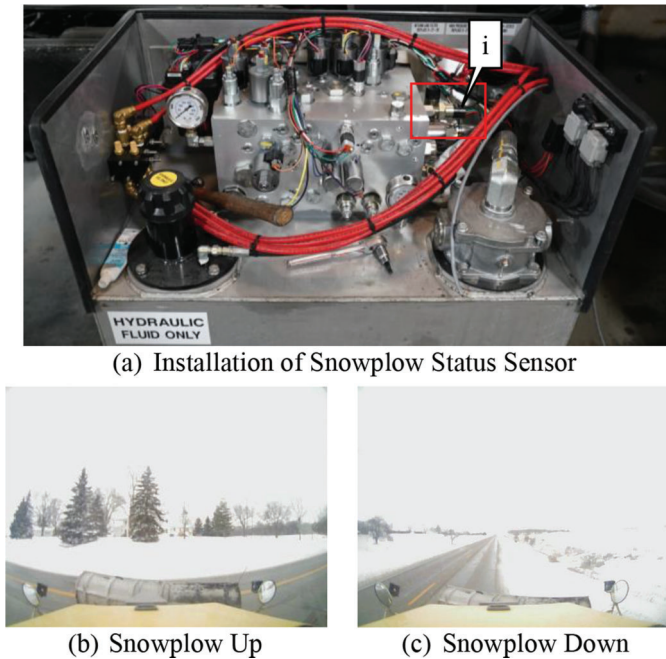


**Figure 4.4** Active plow positions of INDOT trucks.



(a) Testing of Remote Application Prescription



(b) Vendor Remote Support through Virtual Conference Call

**Figure 4.5** Automated granular application testing and deployment.

#### 4.3 Automated Granular Application

Development of automated granular application provides agencies with a method to ensure efficient and consistent application of materials. A field test was performed with an INDOT truck to enable the agency to prescribe application rates remotely. The test confirmed the ability to do so, and further development will be completed to remotely broadcast application rates to fleet vehicles based on MRMS forecasted and current weather conditions. Figure 4.5 shows the steps performed to test and validate the functionality of supplying application rates remotely to the vehicle. Figure 4.5a shows the team in the truck validating the salt spreader values, and Figure 4.5b depicts the team supplying spreader controls to the vehicle from a remote location.

#### 5. WINTER PROBE DATA AFTER ACTION REPORTS

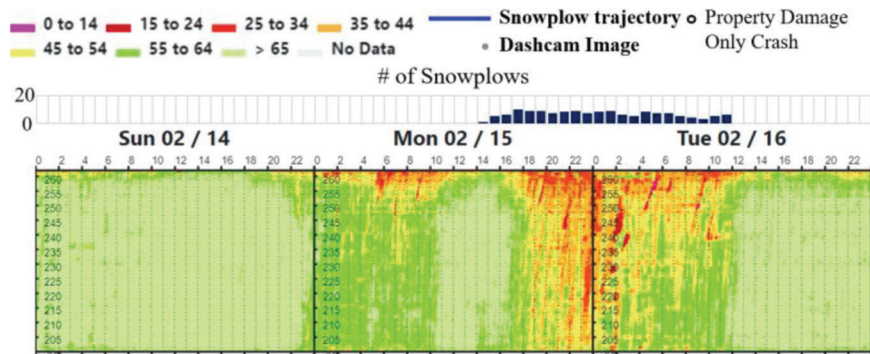
After action reports and performance metrics are essential tools for agencies to evaluate the system performance and understand the impact of a winter storm event (Dao et al., 2019). Travel speeds were monitored over the 2020–2021 winter season along with AVL data captured from the trucks. Vehicle speeds below 45 mph were classified as congested or underperforming during a winter precipitation event. Figure 1.4 shows the congestion profile that was used to provide insight on winter storm impact and deployment measures.

Figure 5.1a shows a time-space diagram (heatmap) colorized by speed for I-65 northbound direction between mile markers 200 and 262 from February 14th to February 16th, 2021. Figure 5.1b includes snowplow trajectories overlaid seen in gray and a blue marker is the interactive feature that allows the user to

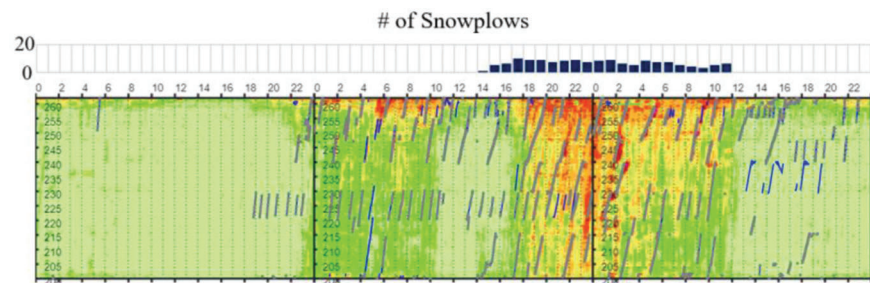
view a truck’s camera image at that point. Figure 5.1c includes crashes extracted from Indiana’s online crash repository. Each crash includes a crash geolocation, timestamp, and manner of collision and are represented at as white markers on the heatmap.

INDOT’s fleet were actively monitoring the storm and accumulation for 4 hours before precipitation began at 10:00 PM on February 14th, 2021. Figure 5.1 shows moderate congestion clearly seen in the northbound direction beginning at 10:00 PM on February 14th, 2021, and more severe congestion experienced at 6:00 PM on February 15th, 2021. Observing traffic speeds and snowplow trajectories shows the impact of snow removal on interstates and that the system did not fully recover until 1:00 PM on February 16th, 2021. These features enhance the agency’s ability to evaluate snow removal processes and best practices.

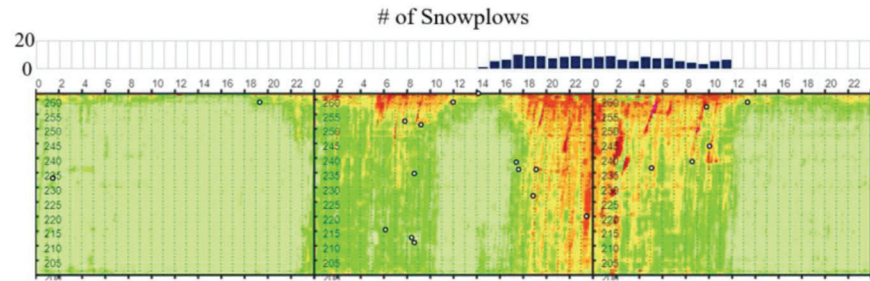
Figure 5.2a shows the heatmap for I-94 westbound from February 14th to 16th, 2021. Beginning at 3:00 PM on February 15th there were several miles of vehicles traveling less than 25 mph across the whole interstate. Callout *i* shows the current location of the vehicle around mile marker 26. Viewing the dash camera of the truck at that time, reveals that tandem activities were performed to transfer snow from the median to the ditch of the highway (Figure 5.2b). This data provided insight to the traffic impact, and this activity was subsequently scheduled at different times of the day to have a lesser impact on traffic. The URL in Figure 5.2 shows an example of the activity performed on I-94 (Desai et al., 2021). Evaluation of snowplow operations was performed over the course of the 2020–2021 winter season and utilizing the AVL data it was found that impact on traffic could be minimized by performing specific operations at off-peak travel time (Desai, Mahlberg, & Bullock, 2021).



(a) I-65 Northbound Heatmap with Vehicle Speeds



(b) I-65 Northbound Heatmap with Vehicle Speeds and Snowplow Trajectories



(c) I-65 Northbound Heatmap with Vehicle Speeds and Crashes

**Figure 5.1** I-65 northbound interstate heatmap for February 14th–16th, 2021.

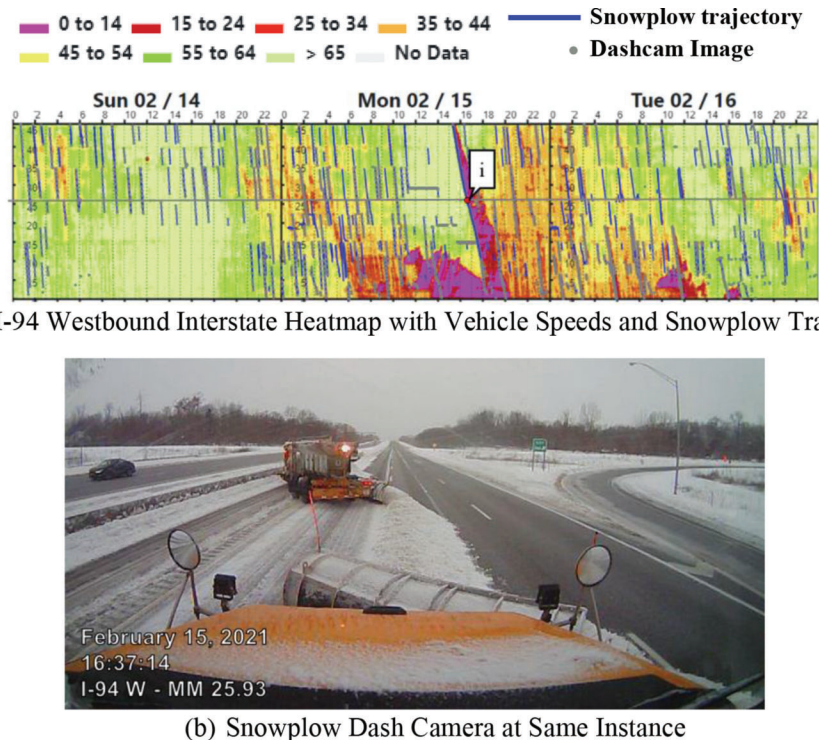


**Figure 5.2** I-94 tandem plowing activities (see <https://doi.org/10.4231/KVTF-W862>).

## 6. AUTOMATED GENERATION OF BRINE PRESCRIPTION BASED ON SHADOW

### 6.1 Motivation

As previously noted, INDOT considers snow and ice removal as their number one priority during the winter (INDOT, 2021). Besides mechanical means, pre- and post-treatments of the road for anti- and de-icing are also among the most effective measures. However, it is common practice today to apply treatments such as brine solutions and various chlorides evenly over long road segments, although it has been long established that road surface in the shade suffers the snow and ice problem significantly more than that under the sun (Bogren & Gustavsson, 1989; Bogren et al., 2000; Millory & Humphreys, 1969; Shao & Lister, 1995). More recently (Hu et al., 2016), applied high-precision Digital Surface Model (DSM) derived from LiDAR data in shading pattern generation for road surface temperature modeling and found that accumulated radiation could better explain measurement results than instantaneous radiation. This LiDAR approach makes it possible to survey large areas in considerable details and accordingly provide dynamic road treatment prescription maps for state-level operations.

In this section, we present an open-source sun-shadow simulator (Zhang, 2021) to generate large-scale dynamic prescription maps for winter road treatment operations. The simulator is written in MATLAB and fully automated for roads in the Indiana State. After the user specifies a road name, a mile marker range for

the segment of interest, and a time range, the simulator is able to do the following.

1. Extract surface polygons for the road segment of interest from public INDOT road information (INDOT, 2016; Indiana Geographic Information Office, 2019).
2. Simulate time- and location-dependent direct sun radiation based on the National Renewable Energy Laboratory (NREL)'s Solar Position Algorithm (SPA) (Reda & Andreas, 2000).
3. Visualize the corresponding dynamic prescription maps in Google Earth for easy user interactions (Google, 2021).

According to our best knowledge, we are the first group combining state-wide road and LiDAR information for large-scale dynamic prescription map generation. Our sun-shadow simulation achieves meter-level precision with a high accuracy. It could precompute the dynamic prescription maps for the whole Indiana State over the winter season as a baseline guidance to increase treatment efficiency and reduce environmental impact (Cooper et al., 2014). Post-treatment actions such as snow and ice removal could also benefit from these maps via proactive workforce deployment and prioritizing high-risk road segments.

### 6.2 Direct-Path Blockage and Normalized Sun Energy

The simulator locates areas in the shade via a direct-path blockage model and estimates local heating effects for regions under the sun via a simplified sun radiation model.

### 6.2.1 Scenario Overview

Figure 6.1 illustrates how the simulator determines whether an observer is in the Sun's shadow given the Sun's position. From the observer's location, a LiDAR z profile is obtained toward the Sun's direction.

For simplicity, the LiDAR z value for the observer is also used as their ground elevation. If any of the LiDAR z samples fall below the direct path between the observer and the Sun, as those for the trees in Figure 6.1, that location is classified as *in the shadow*; otherwise, it is classified as *under the sun*.

Only a limited distance of the LiDAR data, denoted as  $d_{Max}$  in Figure 6.1, needs to be inspected for computational consideration. Increasing  $d_{Max}$  will increase the computation needed for the simulation. However, if  $d_{Max}$  is too low, the accuracy of the simulation may decrease, especially for the case when the sun is at a low angle. For example, obstacles can cause extremely long shadows at sunset/sunrise. These obstacles may be missed with an insufficiently large  $d_{Max}$ .

Suppose we have 12 hours of daylight per day and the daytime solar zenith angle follows a continuous uniform distribution in time with a range between  $-90^\circ$  (sunrise) and  $90^\circ$  (sunset). Then, to ensure no obstacles shorter than  $H_{obs} = 10$  m (a typical three-story building) will be missed except possibly during two time windows of  $T_{win} = 15$  minutes (right after the sunrise and before the sunset, respectively), we would need a distance to inspect,  $d_{Max}$ , such that:

$$\arctan(H_{obs}/d_{Max})/180^\circ \times 12 \text{ h} \times 60 \text{ min/h} = T_{win}$$

With the parameter values above, this gives us:

$$d_{Max} = H_{obs}/\tan(T_{win}/720 \text{ min} \times 180^\circ) \quad (\text{Eq. 6.1})$$

$$= 10 \text{ m}/\tan(15 \text{ min}/720 \text{ min} \times 180^\circ) \gg 152.57 \text{ m}$$

Accordingly,  $d_{Max}$  is set to be 150 m in the simulator.

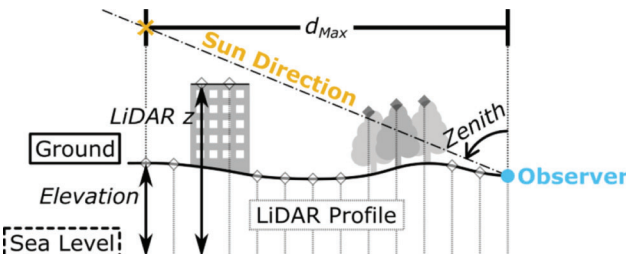


**Figure 6.1** Illustration of the direct-path blockage scenario.

### 6.2.2 Sun's Position and Obstacles

The simulator employs a MATLAB implementation (Mahooti, 2021) of NREL's SPA (Reda & Andreas, 2000) for estimating the solar zenith and azimuth angles based on the date, time, and location on Earth. This algorithm is highly accurate with uncertainties of  $\pm 0.0003^\circ$  in the period from the year -2000 to 6000 (Reda & Andreas, 2000).

The Indiana 2016–2019 Statewide LiDAR data set (Jung & Oh, 2021) was used to locate obstacles including buildings and foliage. LiDAR profiles, as illustrated in Figure 6.1, were generated by linearly interpolating 5-feet-resolution DSM files. A spatial resolution of 1.5 m was chosen to match the DSM resolution.

### 6.2.3 A Simplified Direct Sun Radiation Model

We have assumed that any location of interest with a blocked direct path to the Sun receives no solar radiation. For other locations, as illustrated in Figure 6.2, the absorbed solar power over unit ground area, denoted by  $P$ , can be computed and normalized based on the predicted solar zenith angle,  $\theta$ , from SPA. When  $\theta = 0^\circ$ ,  $P$  peaks at  $P_0$ , and the normalized  $P$ , denoted by  $\hat{P}$ , should peak at one. In general,

$$P \cdot \frac{A}{\cos \theta} = P_0 \cdot A \quad (\text{Eq. 6.2})$$

where  $A$  is a small reference area perpendicular to the Sun's rays. It is worth noting that  $P_0$  does not change significantly throughout the year. Given the maximum and minimum distances,  $r_{Max}$  and  $r_{min}$ , from the Earth to the Sun (Williams, 2020),

$$r_{Max} = 152.099 \times 10^6 \text{ km},$$

$$r_{min} = 147.092 \times 10^6 \text{ km},$$

we can estimate the relationship between the smallest and largest  $P_0$  values,  $P_{0,min}$  and  $P_{0,Max}$ , based on the free-space omnidirectional propagation model:

$$\frac{P_{0,min}}{P_{0,Max}} = \left( \frac{r_{min}}{r_{Max}} \right)^2 \approx 93.5\% \quad (\text{Eq. 6.3})$$

This ratio will be closer to one for the winter season. Thus, we have assumed a constant  $P_0$  value in the simulator. Accordingly, we have defined:

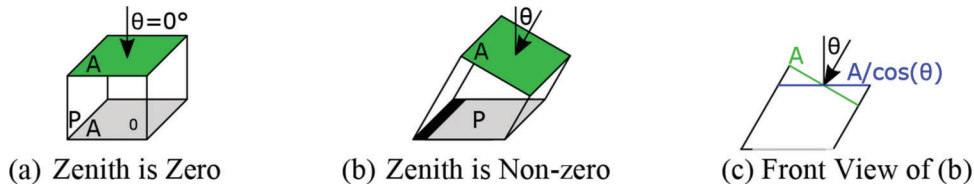


**Figure 6.2** Power computation and normalization based on solar zenith angles.

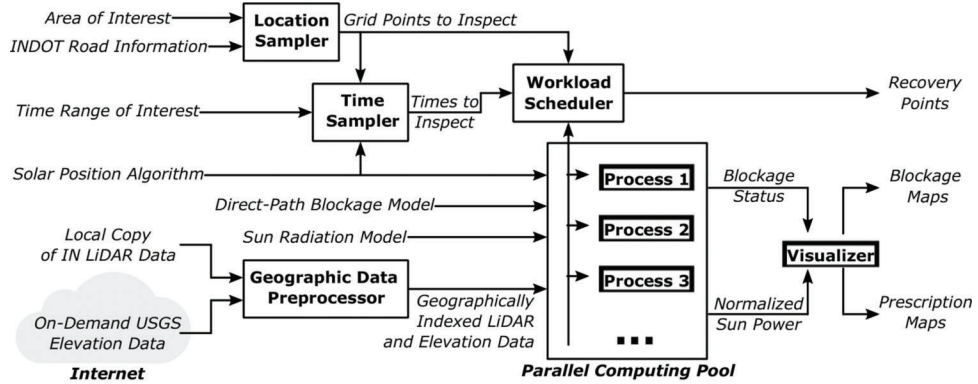


**Figure 6.3** Block diagram of the sun-shadow simulator.

$$\hat{P} = P / P_0 = \cos\theta \quad (\text{Eq. 6.4})$$

With this simplified direct sun radiation model, the simulator is able to estimate the daily solar energy absorbed by unit ground area,  $\hat{E}$ , at a given location via trapezoidal integral of  $\hat{P}$  values at a series of times for the date of interest. Note that  $\hat{E}$  is also a normalized value, where  $\hat{E} = 1$  corresponds to  $E = P_0 \cdot 1\text{d} = P_0 \cdot 24\text{h}$ . Intuitively,  $\hat{E}$  peaking at one represents the maximum amount of solar heat one can get in one day by always staying right under the sun.

### 6.3 Simulator Implementation

This subsection covers the technical details behind the sun-shadow simulator.

#### 6.3.1 Structure Overview

A block diagram is provided in Figure 6.3 as an overview of the simulator's structure. Before any simulation, the geographic data preprocessor processes the local copy of the Indiana DSM (LiDAR-derived) data by geographically indexing the raw files (43,423 .tif files in total; approximately 167 GB in size). This step makes it possible for the simulator to quickly identify the necessary files for any LiDAR profile generation. The preprocessor is also able to download and cache the 1/3rd arc-second terrain elevation data from the United States Geological Services (USGS) as the fallback option for areas not covered by the LiDAR data set.

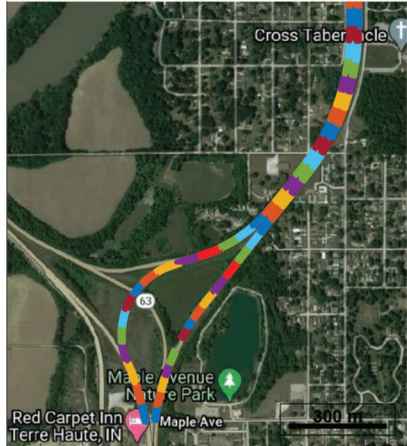
For each simulation, the location and time samplers determine the space-time grid points to consider. After the area/road of interest is specified by the user with a desired spatial resolution, the location sampler generates a grid covering the area accordingly. The location sampler is also able to (1) automatically generate a boundary polygon for the road of interest, and (2) segment the road boundary into small polygons so that the simulation can be carried out by chunk. These procedures require the road information from the

INDOT, including mile markers (INDOT, 2016) and street centerlines (Indiana Geographic Information Office, 2019), as well as a predetermined lane width value. By default, the simulator assumes two-lane roads, creates the road outline with a lane width of 5 m, divides the road into 50-m segments, and generates a grid with a spatial resolution of 3 m for each of the road segment.

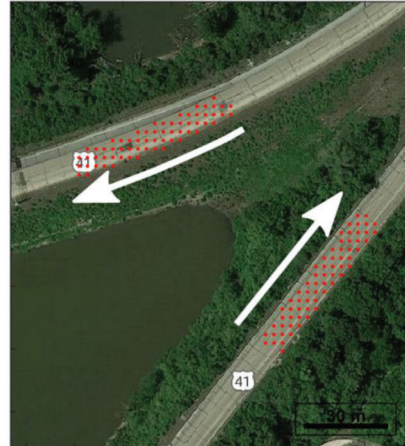
As can be seen in both plots in Figure 6.4, the simulator is flexible enough to work with polygons containing multiple regions and roads with separated lanes. To achieve the results in Figure 6.4a, the simulator generated an interpolation function over available mile markers to translate GPS locations to mile marker values for this road. This converted GPS data points into an ordered set, which was the key to properly breaking sides of the road boundary polygon for smaller road segments. Figure 6.4b shows the 3-m resolution grid for one of the 50-m road segments. As can be seen, the grid points to inspect cover the required road surface.

The time sampler uniformly extracts *times to inspect* from the local time range of interest, based on a desired time resolution for the shadow simulation. It also determines the local time zone for each grid point. This is necessary because roads could extend over multiple time zones but to the operators, the results would be significant as local time. Additionally, for each date covered by the time range of interest, the time sampler takes advantage of SPA to find the sunrise and sunset times for each grid point. Then, it informs the workload scheduler to skip night times accordingly.

The workload scheduler manages the overall simulation progress and periodically generates recovery points in case interruptions occur. The processes in the parallel computing pool compute the simulation based on the direct-blockage and the sun radiation models introduced in Section 6.2. Finally, the visualizer aggregates the sun-shadow status and normalized sun power values from the parallel processes and generates maps for human operators.



(a) Overview of Road Segments



(b) Grid Points for one Segment

**Figure 6.4** Block diagram of the sun-shadow simulator illustrations of the road segmentation and the grid generation procedures for US 41 on Google Maps (Google, n.d.c; plus code: FHWQ+HC Terre Haute, Indiana): (a) From the road name with start and end points of interest, the location sampler automatically locates the road, divides it into small segments, and creates a simulation grid for each segment. (b) Grid points to inspect for one example road segment (50-m long).

### 6.3.2 Simulation Optimization

The following are the techniques we have applied in the sun-shadow simulator to optimize the performance and reduce the computational cost: (1) LiDAR data pre-processing, (2) limiting distance to inspect for obstacles, (3) adjustable time/space resolutions, (4) accurate road polygon generation, (5) skipping times in the night, and (6) parallel computing.

## 6.4 Simulator Performance Evaluation

Multiple experiments have been designed and completed to verify the performance of the simulator. This section highlights two of these to showcase the accuracy of the simulated sun shadow results.

### 6.4.1 On-Campus Tests

Blockages caused by buildings can form distinctive shadows with clear edges for easy comparison with the simulation results. Three photos for the extension of a shadowed area from buildings before the sunset are included in Figure 6.5, along with the corresponding simulation results.

Evidently, the shadowed areas from the simulator align completely with those recorded by the photos. It is worth noting that on Figure 6.5f, there is a narrow swath under the sun on the top of the map, which should instead be in the shade based on Figure 6.5e. However, this is expected because that region is more than  $d_{Max} = 150$  m away from the obstacle, the FLEX building, on the bottom of Figure 6.5f. Increasing the distance to inspect,  $d_{Max}$ , will fix this issue, but as discussed in Section 6.2.1, we chose not to do so considering the extra computational expense.

### 6.4.2 Comparison with Satellite Imagery

The VOSS model photos demonstrate the accuracy for the sun shadow simulator of the blockages caused by buildings over different times, but there is not much foliage in that region of interest. We now simulate the screening effects of trees, which could significantly slow down the melting of snow/ice on the road surface. In Figure 6.6, we look at a segment of SR 35 where there is dense vegetation along both sides. The corresponding sun shadow outputs from the simulator are shown in Figure 6.6b. A perfect match between the simulation results at 1:15 PM and the satellite image can be observed, especially for the shadows cast by the trees on the left side of the road. Accordingly, we can conclude that the satellite image was captured at around 1:15 PM.

## 6.5 Case Study for US 41

The accurate shadow information from the simulator helps in identifying and locating high-risk segments which require more attention during winter road maintenance operations. In this section, we apply the sun-shadow simulator in dynamic prescription map generation for the US 41 segment between Terre Haute and Rockville, Indiana.

### 6.5.1 Identifying Road Sections with Significant Shadows

As illustrated in Figure 6.4, the road has been divided into small segments for high-resolution simulations. However, to quickly find high-risk locations, a low-resolution simulation for points along the road centerline was calculated. To build a grid for this simulation, we (1) split the road surface polygons from the road sampler, such that each resulting polygon has only one

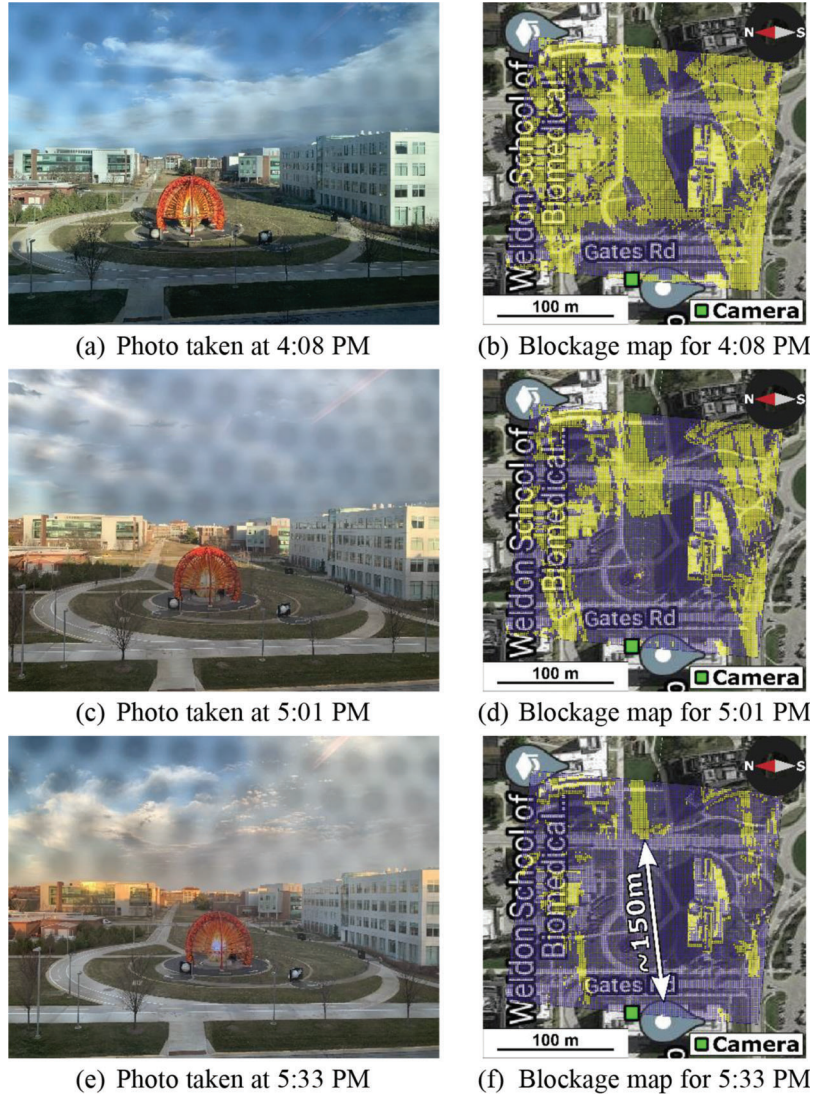


**Figure 6.5** Example photos of building shadows at different times before the sunset, together with simulated blockage status for the same area overlaid on Google Maps (Google, n.d.a; plus code: C3CG+PV West Lafayette, Indiana).

Note: The photos were taken on the 3rd floor of the FLEX Lab building for the VOSS Model at Purdue University on March 11th, 2021. The grey dots on the photos were from the building glass (which should be ignored in the performance evaluation). On the blockage maps, locations in the shade are colored blue while locations under the sun are colored yellow. The perfect match between the photos and the blockage maps proves the high accuracy of the sun-shadow simulator for building blockages at different times.

region, and (2) used the centroids of these polygons. The corresponding results are captured by Figure 6.7. The normalized daily sun energy can be seen in Figure 6.7a. With the help of the empirical CDF of the normalized daily sun energy values, we can conveniently locate the high-risk regions where the received direct sun radiation is limited, as plotted in Figure 6.7b. The locations with the least 10% radiation are plotted as an example.

The low-resolution simulation results can also be used to reduce the computation requirement for large-scale high-resolution simulations. For instance, by carrying out the high-resolution simulations only for the road segment polygons corresponding to the worst

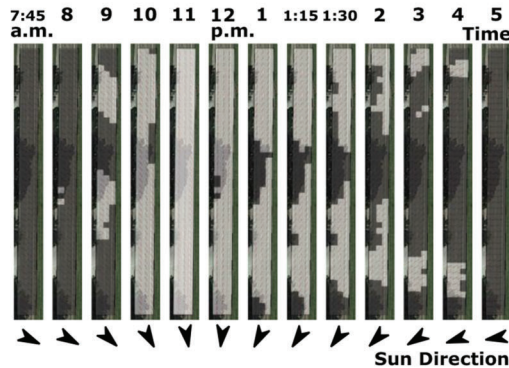
10% locations shown in Figure 6.7b, we can reduce approximately 90% of the overall computation amount planned by the location sampler in Figure 6.4.

#### 6.5.2 High-Resolution Simulation and Treatment Distribution

For a stress test, we repeated the simulations with a 3-m resolution for the whole 38-km road. Figure 6.8 plots the resulting normalized daily sun energy for one 50-m long segment on the date of interest. Based on this information, dynamic prescription maps for variable treatment distribution can be generated. For example, the amount of brine solution needed by one

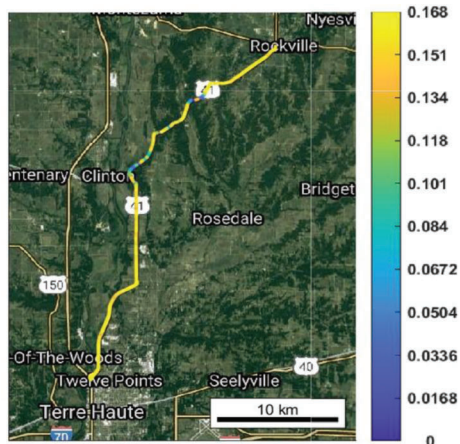


(a) Grid Points for the Area of Interest

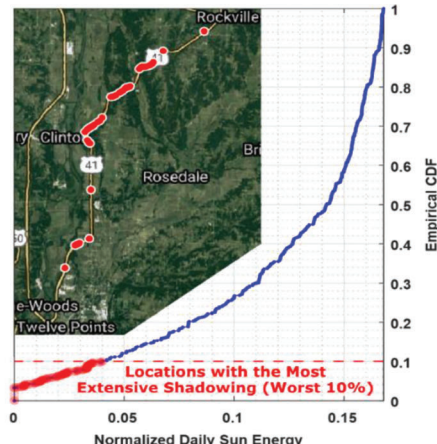


(b) Blockage Maps

**Figure 6.6** Comparison between a satellite image from Google Maps (Google, n.d.b) and blockage results from the simulator. Note: The satellite image was collected on Oct. 7, 2016. The simulation was run for the same date with a 15-minute time resolution. (a) The grid points cover a road segment of 135-m long with a resolution of 3 m. (b) The shape of the shadows from the simulator has a perfect match with the satellite image at around 1:15 PM.



(a) Normalized Daily Sun Energy



(b) The Worst 10% Locations

**Figure 6.7** A set of low-resolution simulations to locate high-risk locations for the 38-km US 41 road segment between Terre Haute and Rockville, Indiana (Google, n.d.c).

Note: The date of interest is Feb. 11th, 2021. The time resolution is 30 min. The spatial resolution for obtaining sample locations along the road is 50 m. (a) The simulation results are aggregated as the normalized daily sun energy on Google Maps—the lower the energy, the higher the risk. (b) The high-risk locations can be easily identified via the empirical CDF.

unit area of the road should be reduced proportionally based on the amount of the sun energy expected to be absorbed.

These high-resolution simulations allow dynamic planning of treatment distribution not only along the road, but also perpendicular to the road along the width side if the equipment allows such fine adjustments. If the treatment is applied by road segment, the simulation results can be aggregated for each segment to create corresponding dynamic prescription maps. For instance, the normalized daily sun energy values for points on the road segment of

interest can be summed up to one value to vary the treatment applied for that segment compared with a reference amount.

For easier access to the large amount of simulation results, the visualizer of our simulator also interfaces with Google Earth (Google, 2021) by exporting desired results into .kml files, as demonstrated by the screenshots in Figure 6.9. Here, the ratio of grid points that are blocked in each road segment polygon is visualized by that polygon's transparency. The left-side *Places* pane in Figure 6.9a has a list of all the blockage status polygons organized in different folders for different

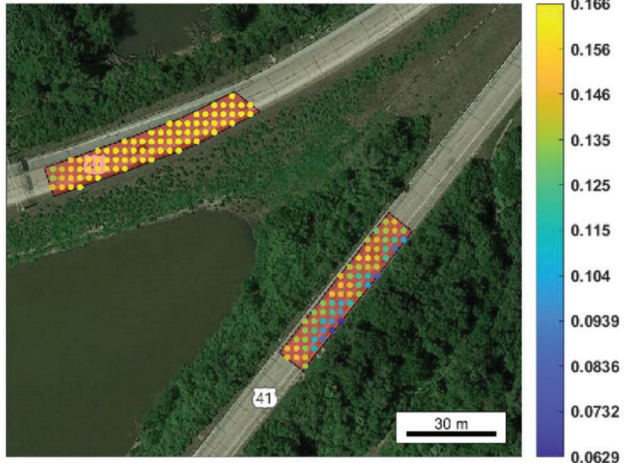
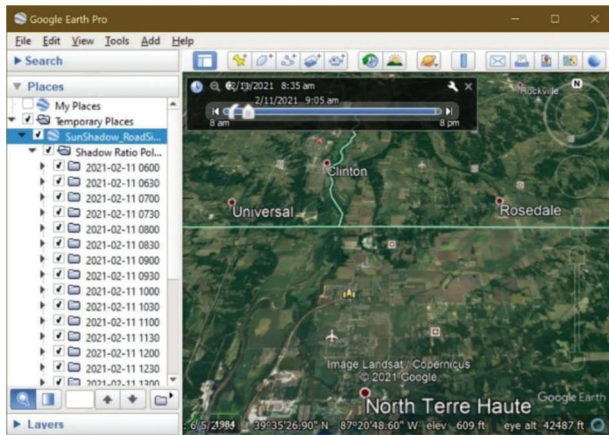
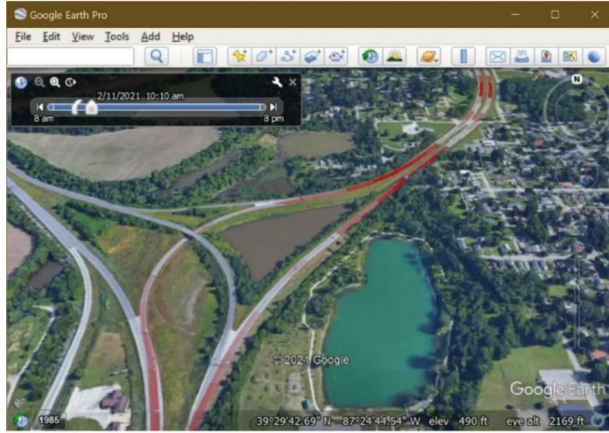


**Figure 6.8** Normalized daily sun energy values overlaid on Google Maps (Google, n.d.c).

Note: The results are for the high-resolution grid of the road segment in Figure 6.4.



(a) Overview



(b) A Zoomed-In View

**Figure 6.9** Simulation results loaded into Google Earth (Google, 2021) for better user interactions.

Note: The transparency of each road segment polygon was proportional to the ratio of unblocked grid points in that polygon. The red polygons are more visible if they have less blocked grid points.

inspected times. The map view, shown in both screenshots, supports common interactions such as zooming and panning. A time bar is also provided on the top for sliding through the simulation results in time. A friendly visualization tool such as this one is the key to ensuring a high usability of the simulator in practice. These maps can be easily extended/improved with extra information, such as the real-time local weather, for a better performance. The simplified sun radiation model in the current simulator can also be updated with more complicated models.

### 6.5.3 Future Work

In the future, we would like to run the simulator for larger road networks. Currently, on a 36-core cluster with 216 GB RAM, the low-resolution (50 m/30 min) simulation introduced in Section 6.5.1 took approximately 3 h to finish, while the high-resolution (3 m/30 min) simulation took approximately 13 days to finish. We will explore the possibility of decreasing the computational requirements by reusing (1) sun position results for nearby locations and (2) prescription maps for the same locations over reasonably short time intervals (e.g., 1 week). We would also like to take into consideration extra information, e.g., the degree of shading, weather, and obstacle types, for more accurate sun radiation results.

## 6.6 Conclusion

Shading significantly slows down the melting process of road snow and ice. High-precision LiDAR data makes it possible to identify the Sun's shadows with high accuracy for large areas at a low cost. In this paper, we present a fully automated sun-shadow model to locate sections of road with the highest amount of shadowing. The resulting dynamic prescription maps are flexible, user-friendly, and could guide road treatment for improved efficiency with reduced environmental impact.

## 7. RESULTS, SUMMARY, AND RECOMMENDATIONS

This report summarizes the work performed to develop an intelligent automated snowplow across Indiana. The automated brining system was deployed on two 5,500-gallon tankers and used on I-70, I-74, and I-465 during the 2020–2021 winter season after successful testing on a sidewalk prototype. In addition, calibration workshops and trainings were hosted in all 6 districts in the state that involved new techniques to improve the calibration process. Furthermore, AVL systems that reported real-time location information with camera images and application rates were deployed on all INDOT snowplows and this data was used to evaluate winter operations during the 2020–2021 winter season.

The findings of this research were as follows.

1. Calibration of salt spreaders is important to ensure that proper amount of salt is delivered to the roadway. The team developed and demonstrated new calibration techniques and methods, reducing material usage and labor needed to calibrate vehicles. Figure 1.1a shows the use of the new calibration box and Figure 1.1b illustrates the calibration workshops held at each district. The video link in Figure 1.1 shows a time-lapse at the Crawfordsville calibration workshop and the complete calibration of a truck completed in 22 minutes.
2. When anti-icing chemicals are applied to bridge decks, the driver must turn on and off the application at each bridge. One pass on a single lane in one direction requires the driver to turn on and off the brine application approximately 100 times. Depending upon traffic and driver workload, some applications zones may be missed so there is variation in the number of spray zones on between runs (Table 1.1). The team developed and scaled an automated precision brine applicator on two 5,500-gallon tankers (Figure 3.3) to reduce driver workload and potential for distracted driving.
3. Effectively managing plow trucks during a winter storm requires having good knowledge of where the trucks are so that resources can be most effectively allocated. The project team successfully integrated telematics from 1,100 trucks into real-time dashboards. Figure 5.1 shows a time-space diagram (heatmap) colorized by speed for I-65 northbound direction between mile markers 200 and 262 from February 14th to February 16th, 2021. Snowplow trajectories are overlaid on the heatmap to show snow removal activities with respect to traffic speeds. Additionally, to provide context to winter operation procedures statewide, Figure 1.7a illustrates interstate traffic speeds, weather radar, truck locations and applied materials on the roadway surfaces. A video of operations during the storm can be found in Figure 1.7. This dashboard allows operation managers to analyse storm impact and effectively deploy trucks. Figure 1.7b shows the interactive feature of the dashboard and the ability for the user to select a truck to determine location information and view the dash camera image.
4. Development of after-action winter storm reports to provide agencies with data-driven decisions and training. This information will provide agency management with insight on deployment and evaluation measures of each precipitation event. Figure 1.4a illustrates vehicle speeds operating below 45 mph on Indiana Interstates from January 18 to February 16th, 2021. Figure 1.4b shows the deployed snowplows during that same interval.
5. Generation of large-scale dynamic prescription maps for winter road treatment operations utilizing sun-shadow simulation. These prescription maps provide agencies with a tool to increase treatment efficiently, reduce environmental impact and prioritize high-risk road segments.

## Recommendations

1. Training and implementation of calibration practices should be continued to provide accurate data and ensure correct application amounts.

2. Continued implementation and installation of automated precision controllers fleetwide to reduce driver distraction and provide consistent pre-treatment measures.
3. Further testing and data validation with the telematic installer to ensure accurate data readings and evaluations.
4. Develop training materials to provide agency operators and managers tools to determine operation best-practices and deployment.
5. Perform the simulation tests on larger road networks and include additional information including degree of shading, weather, and obstacle types to present more accurate sun radiation results.

## REFERENCES

- Bogren, J., & Gustavsson, T. (1989). Modelling of local climate for prediction of road slipperiness. *Physical Geography*, 10(2), 147–164. <https://doi.org/10.1080/02723646.1989.10642374>
- Bogren, J., Gustavsson, T., Karlsson, M., & Postgård, U. (2000). The impact of screening on road surface temperature. *Meteorological Applications*, 7(2), 97–104. <https://doi.org/10.1017/S135048270000150X>
- Breining, G. (2017). We're pouring millions of tons of salt on roads each winter. *Ensia*. <https://ensia.com/features/road-salt/>
- Brennan, T. M., Jr., Remias, S. M., Grimmer, G. M., Horton, D. K., Cox, E. D., & Bullock, D. M. (2013). Probe vehicle-based statewide mobility performance measures for decision makers. *Transportation Research Record*, 2338(1), 78–90. <https://doi.org/10.3141/2338-09>
- Cooper, C. A., Mayer, P. M., & Faulkner, B. R. (2014). Effects of road salts on groundwater and surface water dynamics of sodium and chloride in an urban restored stream. *Biogeochemistry*, 121(1), 149–166. <https://doi.org/10.1007/s10533-014-9968-z>
- Dao, B., Hasanzadeh, S., Walker, C. L., Steinkruger, D., Esmaeili, B., & Anderson, M. R. (2019). Current practices of winter maintenance operations and perceptions of winter weather conditions. *Journal of Cold Regions Engineering*, 33(3), 04019008. [https://doi.org/10.1061/\(asce\)cr.1943-5495.0000191](https://doi.org/10.1061/(asce)cr.1943-5495.0000191)
- Day, C. M., McNamara, M. L., Li, H., Sakhare, R. S., Desai, J., Cox, E. D., Horton, D. K., & Bullock, D. M. (2016). *2015 Indiana mobility report and performance measure dashboards*. <https://doi.org/10.5703/1288284316352>
- Desai, J., Mahlberg, J., & Bullock, D. M. (2021). *Intelligent snow plow: February 5, 2021 Windrow Activities*. Purdue University Research Repository. <https://doi.org/10.4231/KVTF-W862>
- Desai, J., Mahlberg, J., Kim, W., Sakhare, R., Li, H., McGuffey, J., & Bullock, D. M. (2021) Leveraging telematics for winter operations performance measures and tactical adjustment. *Journal of Transportation Technologies*, 11(4), 611–627. <https://doi.org/10.4236/jtt.2021.114038>
- FHWA. (2020). *How do weather events impact roads?* [Webpage]. Federal Highway Administration. [https://ops.fhwa.dot.gov/weather/q1\\_roadimpact.htm](https://ops.fhwa.dot.gov/weather/q1_roadimpact.htm)
- Fitch, G. M., Smith, J. A., & Clarens, A. F. (2013). Environmental life-cycle assessment of winter maintenance treatments for roadways. *Journal of Transportation Engineering*, 139(2), 138–146. [https://doi.org/10.1061/\(ASCE\)TE.1943-5436.0000453](https://doi.org/10.1061/(ASCE)TE.1943-5436.0000453)

- Google. (n.d.a). [Purdue Campus in West Lafayette, IN]. Google Maps. Retrieved March 11, 2021, from <https://goo.gl/maps/9cg8BHW2tw97196U6>
- Google. (n.d.b). [US 35 in Winamac, IN]. Google Maps. Retrieved April 7, 2021, from <https://goo.gl/maps/9cg8BHW2tw97196U6>
- Google. (n.d.c). [US 41 road segment between Terre Haute and Rockville, Indiana]. Google Maps. Retrieved April 13, 2021, from <https://goo.gl/maps/9cg8BHW2tw97196U6>
- Google. (2021). Google Earth LLC. <https://www.google.com/earth/>
- Hounsell, N., & McLeod, F. (1998). Automatic vehicle location: Implementation, application, and benefits in the United Kingdom. *Transportation Research Record*, 1618(1), 155–162. <https://doi.org/10.3141/1618-19>
- Hu, Y., Almkvist, E., Lindberg, F., Bogren, J., & Gustavsson, T. (2016). The use of screening effects in modelling route-based daytime road surface temperature. *Theoretical and Applied Climatology*, 125(1–2), 303–319. <https://doi.org/10.1007/s00704-015-1508-9>
- Indiana Geographic Information Office. (2019, December 11). *Street centerlines maintained by county agencies in Indiana* [Dataset]. [http://maps.indiana.edu/download/Infrastructure/Streets\\_Centerlines\\_IGIO.zip](http://maps.indiana.edu/download/Infrastructure/Streets_Centerlines_IGIO.zip)
- INDOT. (2016, July 1). *Mile-marker reference post inventory for roads in Indiana, 2015*. Indiana Department of Transportation. [https://maps.indiana.edu/download/Infrastructure/Interstates\\_Mile\\_Markers\\_System1\\_INDOT.zip](https://maps.indiana.edu/download/Infrastructure/Interstates_Mile_Markers_System1_INDOT.zip)
- INDOT. (2021). *Winter operations* [Webpage]. Indiana Department of Transportation. <https://www.in.gov/indot/3222.htm>
- Jung, J., & Oh, S. (2021). *Indiana statewide normalized digital height model (2016–2019)*. Purdue University Research Repository. <https://doi.org/10.4231/QAA5-6J29>
- Mahlberg, J., Jewison, M., Bell, J., & Bullock, D. M. (2021). *Intelligent snow plow: Calibration workshop training timelapse*. Purdue University Research Repository. <https://doi.org/10.4231/XBET-8A88>
- Mahooti, M. (2021). *NREL's Solar Position Algorithm (SPA)*. MATLAB Central File Exchange. <https://www.mathworks.com/matlabcentral/fileexchange/59903-nrel-solar-position-algorithm-spa>
- Millory, M. H., & Humphreys, J. S. (1969). *The influence of topography on the duration of ice-forming conditions on a road surface* (Report No. Rrl-LR-274). Highway Safety Literature. <https://trid.trb.org/view/114954>
- Nixon, W. A., & Qiu, L. (2005). Developing a storm severity index. *Transportation Research Record*, 1911(1), 143–148. <https://doi.org/10.3141/1911-14>
- Parker, S. K., & Skitmore, M. (2005). Project management turnover: Causes and effects on project performance. *International Journal of Project Management*, 23(3), 205–214. <https://doi.org/10.1016/j.ijproman.2004.10.004>
- Raven Applied Technology. (2020). *Field computers* [Webpage]. Retrieved April 11, 2020, from <https://ravenprecision.com/products/field-computers>
- Reda, I., & Andreas, A. (2008, January). *Solar position algorithm for solar radiation applications* (Report No. NREL/TP-560-34302). National Renewable Energy Laboratory. <https://www.nrel.gov/docs/fy08osti/34302.pdf>
- Sakhare, R., Mahlberg, J., Desai, J., Kim, W., Li, H., & Bullock, D. M. (2021). *Intelligent snow plow: February 15, 2021 winter storm activity*. Purdue University Research Repository. <https://doi.org/10.4231/R3XJ-0875>
- Shao, J., & Lister, P. J. (1995). The prediction of road surface state and simulation of the shading effect. *Boundary-Layer Meteorology*, 73(4), 411–419. <https://doi.org/10.1007/BF00712680>
- Van Sickle, J. (2021). *Real-time kinematic and differential GPS*. Penn State College of Earth and Mineral Sciences. <https://www.e-education.psu.edu/geog862/node/1828>
- Williams, D. R. (2020). *Earth fact sheet*. NASA Goddard Space Flight Center. <https://nssdc.gsfc.nasa.gov/planetary/factsheet/earthfact.html>
- Zhang, Y. (2021). *Sun shadow simulator*. GitHub. <https://github.com/YaguangZhang/SunShadowSimulatorMatlabWorkspace>

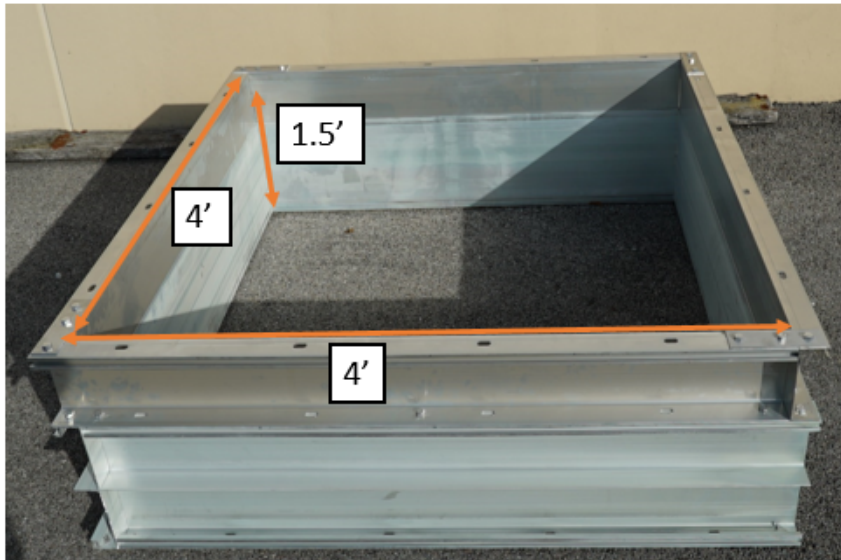
## **APPENDICES**

### **Appendix A. Innovative Calibration Techniques**

### **Appendix B. Summary of Training Materials**

## APPENDIX A. INNOVATIVE CALIBRATION TECHNIQUES

### Calibration Bin Dimension and Calculations



$$\text{Volume of Calibration Box} = 1.5' \times 4' \times 4' = 24 \text{ ft}^3$$

$$\text{Assumed Density of Salt} = 80 \frac{\text{lb}}{\text{ft}^3}$$

$$\text{Approximate Weight of Salt in Bin} = 24 \text{ ft}^3 \times 80 \frac{\text{lb}}{\text{ft}^3} = 1,920 \text{ lbs}$$

		<p><b>Benefits:</b></p> <ul style="list-style-type: none"> <li>• Calibration Completed Onsite</li> <li>• *Average Calibration time decrease by 1-2 hours</li> </ul> <small>*Value achieved by questioning users</small>
		<p><b>Point of Contact:</b></p> <p><b>Jeremy McGuffey</b> Indiana Department of Transportation Email: <a href="mailto:jmcguffey@indot.in.gov">jmcguffey@indot.in.gov</a> Office: (317) 234-5665</p>
		<p><b>Darcy Bullock</b> Purdue University Email: <a href="mailto:darcy@purdue.edu">darcy@purdue.edu</a></p> <p><b>Justin Mahlberg</b> Purdue University Email: <a href="mailto:jmahlber@purdue.edu">jmahlber@purdue.edu</a></p>

Figure A.1 One page calibration reference guide.

## APPENDIX B. SUMMARY OF TRAINING MATERIALS

Table B.1 Training Videos for Calibration, Automated Brine Application, and Winter Storm Impact/Deployment Measures

Title	Link
How to Calibrate a Muncie Advantage+ Controller	<a href="https://doi.org/10.4231/9S3K-9J39">https://doi.org/10.4231/9S3K-9J39</a>
How to Calibrate a Certified Power Freedom 2 Controller	<a href="https://doi.org/10.4231/7015-1X74">https://doi.org/10.4231/7015-1X74</a>
How to Calibrate a Muncie Omni Controller	<a href="https://doi.org/10.4231/CRCY-FF55">https://doi.org/10.4231/CRCY-FF55</a>
How to Calibrate a FORCE America 5100ex Controller	<a href="https://doi.org/10.4231/NEY0-9F04">https://doi.org/10.4231/NEY0-9F04</a>
Calibration Workshop Training	<a href="https://doi.org/10.4231/XBET-8A88">https://doi.org/10.4231/XBET-8A88</a>
How to Calibrate the Calibration Box	<a href="https://doi.org/10.4231/RNV9-8F21">https://doi.org/10.4231/RNV9-8F21</a>
Importance of Brine	<a href="https://doi.org/10.4231/MECJ-AN70">https://doi.org/10.4231/MECJ-AN70</a>
Automated Precision Brine Application	<a href="https://doi.org/10.4231/X34H-9Z21">https://doi.org/10.4231/X34H-9Z21</a>
February 15th, 2021, Winter Storm Activity	<a href="https://doi.org/10.4231/R3XJ-0875">https://doi.org/10.4231/R3XJ-0875</a>
February 10th, 2021, Winter Storm Activity	<a href="https://doi.org/10.4231/RR0D-C529">https://doi.org/10.4231/RR0D-C529</a>
February 8th, 2021, Winter Storm Activity	<a href="https://doi.org/10.4231/VXZQ-9G72">https://doi.org/10.4231/VXZQ-9G72</a>
December 16th, 2021, Winter Storm Activity	<a href="https://doi.org/10.4231/7DSJ-1475">https://doi.org/10.4231/7DSJ-1475</a>
February 8th, Tandem Plow Activities	<a href="https://doi.org/10.4231/A0BA-P609">https://doi.org/10.4231/A0BA-P609</a>
February 6th, Tow Plow Activities	<a href="https://doi.org/10.4231/8KER-F373">https://doi.org/10.4231/8KER-F373</a>
February 5th, Tandem Plow Windrow Activities	<a href="https://doi.org/10.4231/KVTF-W862">https://doi.org/10.4231/KVTF-W862</a>
How to Use Parsons Tablet	<a href="https://doi.org/10.4231/WC1P-N150">https://doi.org/10.4231/WC1P-N150</a>
Integrated Connected Vehicle Data and INDOT Snowplow 63678 Telematics Feed from February 15th–16th, 2021, Winter Storm	<a href="https://doi.org/10.4231/D8XT-JS45">https://doi.org/10.4231/D8XT-JS45</a>
Integrated Connected Vehicle Data and INDOT Snowplow 63550 Telematics Feed from February 15th–16th, 2021, Winter Storm	<a href="https://doi.org/10.4231/V572-YX70">https://doi.org/10.4231/V572-YX70</a>
Integrated Connected Vehicle Data and INDOT Traffic Camera Feed from February 15–16th, 2021, Winter Storm	<a href="https://doi.org/10.4231/SFMN-R881">https://doi.org/10.4231/SFMN-R881</a>

## About the Joint Transportation Research Program (JTRP)

On March 11, 1937, the Indiana Legislature passed an act which authorized the Indiana State Highway Commission to cooperate with and assist Purdue University in developing the best methods of improving and maintaining the highways of the state and the respective counties thereof. That collaborative effort was called the Joint Highway Research Project (JHRP). In 1997 the collaborative venture was renamed as the Joint Transportation Research Program (JTRP) to reflect the state and national efforts to integrate the management and operation of various transportation modes.

The first studies of JHRP were concerned with Test Road No. 1—evaluation of the weathering characteristics of stabilized materials. After World War II, the JHRP program grew substantially and was regularly producing technical reports. Over 1,600 technical reports are now available, published as part of the JHRP and subsequently JTRP collaborative venture between Purdue University and what is now the Indiana Department of Transportation.

Free online access to all reports is provided through a unique collaboration between JTRP and Purdue Libraries. These are available at <http://docs.lib.purdue.edu/jtrp>.

Further information about JTRP and its current research program is available at <http://www.purdue.edu/jtrp>.

## About This Report

An open access version of this publication is available online. See the URL in the citation below.

Mahlberg, J., Zhang, Y., Jha, S., Mathew, J. K., Li, H., Desai, J., Kim, W., McGuffey, J., Wells, T., Krogmeier, J. V., & Bullock, D. M. (2021). *Development of an intelligent snowplow truck that integrates telematics technology, roadway sensors, and connected vehicle* (Joint Transportation Research Program Publication No. FHWA/IN/JTRP-2021/27). West Lafayette, IN: Purdue University.  
<https://doi.org/10.5703/1288284317355>